

# A portable LED-based diamond magnetometer for outreach and teaching labs

Hollis Williams<sup>1,2</sup>, Alex Newman<sup>1</sup>, Stuart Graham<sup>1</sup>, Colin Stephen<sup>1</sup>, Gavin Morley<sup>1</sup>

<sup>1</sup>Department of Physics, University of Warwick, Coventry CV4 7AL, United Kingdom

<sup>2</sup>Current address: Theoretical Sciences Visiting Program, Okinawa Institute of Science and Technology Graduate University, Onna 904-0495, Japan

Contact: [gavin.morley@warwick.ac.uk](mailto:gavin.morley@warwick.ac.uk), [holliswilliams@hotmail.co.uk](mailto:holliswilliams@hotmail.co.uk)

## Abstract

We present a compact, low-cost version of an NV center diamond magnetometer which replaces the standard green laser with a high-power LED. This modification improves safety, reduces cost, and allows the green excitation and red photoluminescence to be viewed directly during demonstrations. The device is simple to assemble and suitable for outreach activities and undergraduate laboratories. We show that it can produce ODMR spectra and respond to nearby magnetic objects, with a sensitivity on the order of  $1 \mu\text{T}/\sqrt{\text{Hz}}$ . Supplementary material provides details of the construction and suggestions for student investigations to support use in teaching laboratories.

## 1 Introduction

The rapid growth of quantum technology has created a demand for quantum teaching labs and demonstrations at undergraduate level. NV (nitrogen vacancy) centers in diamond are appealing for such demonstrations, because they are stable qubits at room temperature and can be used to study a range of quantum phenomena [1, 2]. They also have various applications in quantum computing and magnetic sensing. Through optically detected magnetic resonance (ODMR), students can visualize spin-state dynamics, Zeeman splitting, and basic magnetometry principles.

Several recent works have outlined teaching experiments based on the physics of the NV center and provide simplified designs suitable for undergraduate-level laboratories [18]. Stegemann et al. demonstrated a modular, mostly 3D-printed ODMR apparatus which uses micro-sized NV diamonds and inexpensive electronics, enabling a complete experiment for well under €250 [4]. Similarly, the open-source Uncut Gem platform from Quantum Village provides a modular NV magnetometer which relies on easily available components and minimal optics [5, 6]. These designs offer highly affordable routes for observing ODMR spectra and so represent the cheapest possible options for introducing the physics of the NV center into teaching laboratories.

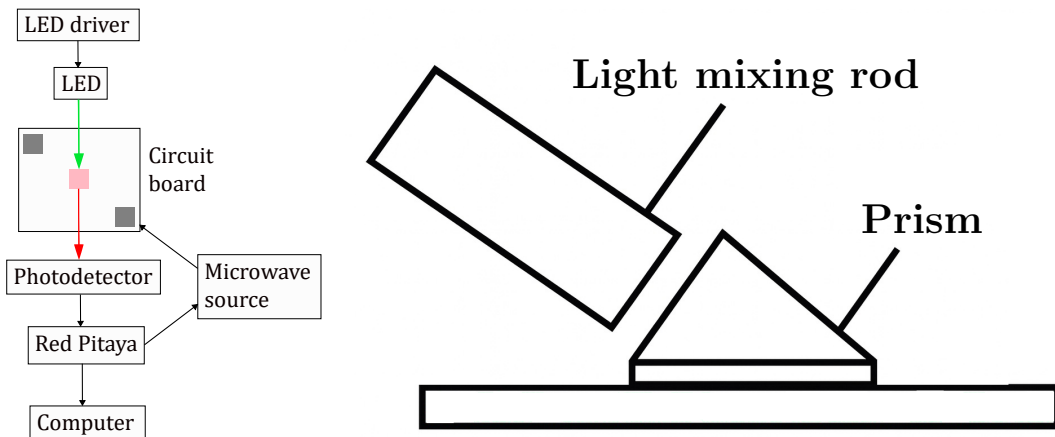


Figure 1: (Left) Schematic of the experiment. The gray squares denote the two block magnets attached to the circuit board and the pink square denotes the NV diamond. (Right) Schematic of the prism and diamond placement (not to scale). The bottom rectangle denotes the circuit board and the rectangle between the prism and the circuit board is the NV diamond placed on top of a thin metal pad. The gap between the prism and the light mixing rod is exaggerated to indicate that a filter is placed in between.

In this Note, we present a portable NV magnetometer which uses a high-power green LED instead of a laser. This magnetometer prioritizes safety, portability, reliable performance, and direct visualization for outreach and undergraduate settings. Although it does not reach the affordability of the very low cost modular options which are available in the literature, the magnetometer which we present here is tailored for teaching and outreach environments where clarity of the fluorescence signal and ease and reliability of the demonstration are essential. The use of an LED reduces enables both the green excitation and red photoluminescence to be seen with the naked eye, which is especially effective in public demonstrations. Low power (few-milliwatt) 532 nm laser modules can also be used in teaching-lab implementations of ODMR experiments, LED illumination requires no laser safety procedures or alignment, making it particularly suitable for outreach demonstrations and environments with minimal supervision.

Although the magnetometer is not as low-cost as the modular options described above, the design remains inexpensive compared to laboratory laser systems and yields robust fluorescence signals from a millimetre-scale NV-rich diamond. Despite its simplicity, the LED device produces clear ODMR spectra and can detect changes in the local magnetic environment with a sensitivity of around  $1 \mu\text{T}/\sqrt{\text{Hz}}$ . We provide a concise description of the operating principles and demonstration capabilities of the apparatus, with detailed assembly instructions, schematics, and example data provided in the Supplementary Material.

## 2 Concept and Demonstration

The central idea of the device is to use a high-power green LED to excite a millimetre-scale diamond containing a high concentration of  $\text{NV}^-$  centers, and to detect the resulting red

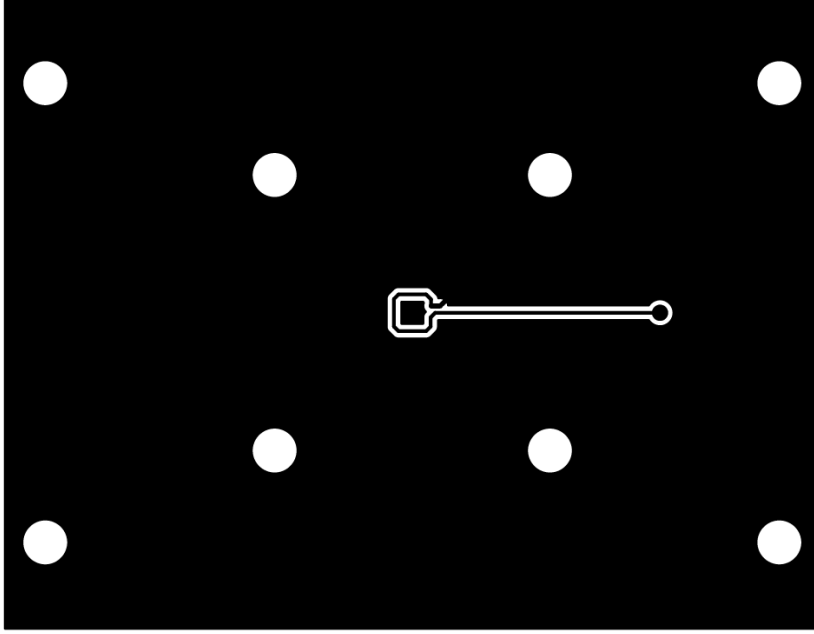


Figure 2: Excerpt of the top copper Gerber layer of the printed circuit board showing the integrated microwave loop used for ODMR. The circular pad on the right connects to the SMA input. A straight copper trace routes the microwave signal to the printed single-turn loop in the middle of the board, which generates the oscillating magnetic field to drive the NV spin transitions. The diamond sits directly above this loop during operation. Full PCB design files are provided in the Supplementary Material.

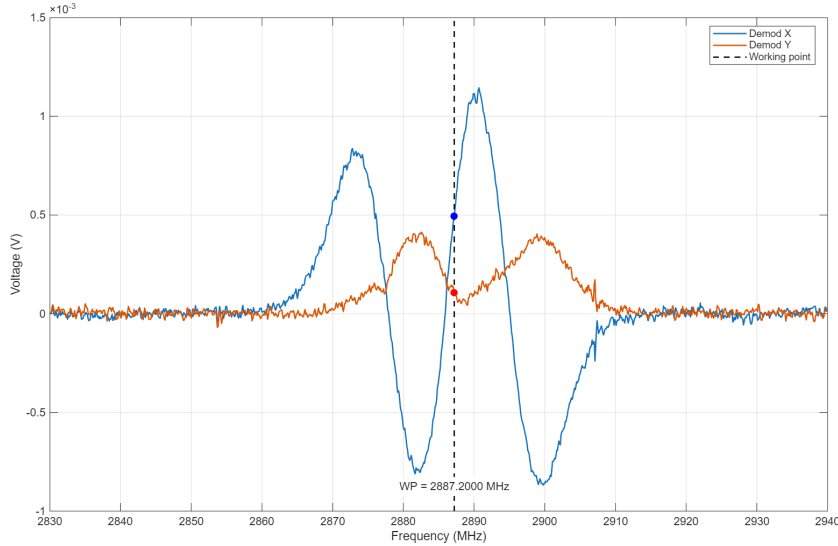


Figure 3: Measured ODMR spectrum from the LED-excited diamond magnetometer, acquired using the same operating settings as the demonstration in Fig. 5. The dashed line marks the working point, defined as the frequency at which the ODMR amplitude exhibits its maximum slope  $dV/df$ .

photoluminescence (PL) while applying microwave radiation near the NV spin resonances. A simplified schematic of the optical and electronic layout is shown in Fig. 1(a). The LED output is fed into a short hexagonal light-mixing rod, which homogenizes the illumination and delivers it to a right-angle prism. The prism directs the green light onto the diamond mounted on the printed circuit board, whilst simultaneously collecting the red photoluminescence and returning it through the rod to a long-pass filter and amplified photodiode. Since the green excitation and red fluorescence are both easily visible to the naked eye, students can directly observe the physical processes responsible for the ODMR signal.

To clarify the optical and mechanical interface on the circuit board, Fig. 1(b) provides a detailed view of the prism-rod-diamond assembly. The diamond is bonded to a reflective metal pad on the board, the prism is placed on top of the diamond, and the face of the mixing rod is aligned so that it presses against the face of the prism. This compact geometry provides efficient PL collection without the need for lenses and keeps alignment requirements minimal. The board incorporates a printed single-turn loop antenna which provides the oscillating magnetic field required for ODMR. The loop is etched into the top copper layer and is driven from the SMA connector through a short copper transmission line, as shown in Fig. 2. The diamond is positioned directly above the loop to ensure strong near-field coupling. An excerpt of the top copper layer is included in the figure for clarity, and the full Gerber files are available in the Supplementary Material.

Microwave excitation for ODMR is supplied by a compact module. In continuous-wave operation, the LED is held at constant intensity whilst the microwave frequency is swept. When the microwave field is resonant with the  $|m_s = 0\rangle \rightarrow |m_s = \pm 1\rangle$  transitions, the PL decreases, producing an ODMR dip in the fluorescence. With a bias magnetic field supplied by two small permanent magnets, the degeneracy of the  $|m_s = \pm 1\rangle$  states is lifted and a pair of resonances is observed. A representative ODMR spectrum obtained with the LED magnetometer is shown in Fig. 3. The spectrum was recorded using the same operating configuration as the magnetometer demonstration (identical LED driver setting, microwave source power, and Red Pitaya lock-in configuration), ensuring that it reflects the actual working conditions of the device. The demodulated X-channel exhibits the characteristic dispersive line shape with two resonances corresponding to different NV orientations under the applied bias field, whereas the Y-channel remains close to zero. We indicate the magnetometer working point by marking the frequency at which the ODMR amplitude has the largest slope  $dV/df$ , which maximizes magnetic field responsivity.

The magnetometer has been used successfully in outreach activities. The entire setup packs into two small plastic boxes and can be reassembled in a few minutes (shown in Fig. 4). At a recent event in our Physics Department, students viewed the PL signal on a laptop whilst magnetic objects were brought near the sensor. For simple demonstrations, it is sufficient to observe the raw PL signal, which changes visibly in response to nearby magnetic objects. Fig. 5 shows the demodulated PL signal whilst a steel Allen key was moved close to the magnetometer. It can be seen that a spike forms as the object is brought near, giving a compelling demonstration that the device functions as a magnetometer.

For more quantitative laboratory use, full ODMR spectra can be acquired by scanning the microwave frequency as described above. Additional details on the circuit board, a complete parts list with prices, CAD files, and the sensitivity characterization of the magnetometer are provided in the Supplementary Material.

### 3 Conclusion

We have presented a portable NV center magnetometer which uses LED illumination instead of a laser, making it especially suitable for outreach and undergraduate laboratory settings. The device produces clear ODMR spectra and responds visibly to nearby magnetic objects, enabling both qualitative demonstrations and quantitative measurements. During outreach events the magnetometer proved easy to assemble and operate, with students able to observe its response in real time. In an instructional laboratory, the system can support introductory activities, as well as more advanced exercises involving magnet alignment, bias-field estimation, or parameter optimisation.

### Author Declarations

The authors have no conflicts to disclose.

### Acknowledgments

Alex Newman’s PhD studentship is funded by an EPSRC iCASE award to UKNNL (United Kingdom National Nuclear Laboratory). This work received funding from the National Nuclear Laboratory’s Science and Technology programme (Decontamination and Decommissioning Core Science). This work is also supported by Innovate UK grant 10003146, EPSRC grant EP/V056778/1 (Prosperity Partnership with Element Six), an EPSRC Impact Acceleration Account (IAA) award, the EPSRC Q-BIOMED Hub EP/Z533191/1, the EPSRC Quantum Computation and Simulation Hub EP/T001062/1, and STFC grant number ST/W006561/1. This research is funded in part by the Gordon and Betty Moore Foundation through Grant GBMF12328, DOI 10.37807/GBMF12328. This material is based upon work supported by the Alfred P. Sloan Foundation under Grant No. G-2023-21130.

### References

- [1] V.K. Sewani, H.H. Vallabhapurapu, Y. Yang, H.R. Firgau, C. Adambukulam, B.C. Johnson, J.J. Pla and A. Laucht, Coherent control of  $NV^-$  in a quantum teaching lab, *Am. J. Phys.* **88**, 1156-1169 (2020).
- [2] Z. Yuan, S. Mukherjee, J.D. Thompson, N.P. de Leon, A. Gardill and S. Kolkowitz, An instructional lab apparatus for quantum experiments with single nitrogen-vacancy centers in diamond, *Am. J. Phys.* **92**, 892-900 (2024).
- [3] H. Zhang, C. Belvin, W. Li, J. Wang, J. Wainwright, R. Berg and J. Bridger, Little bits of diamond: Optically detected magnetic resonance of nitrogen-vacancy centers, *Am. J. Phys.* **86**, 225-236 (2018).
- [4] J. Stegemann et al., Modular low-cost 3D printed setup for experiments with NV centers in diamond, *Eur. J. Phys.* **44**, 035402 (2023).

[5] <https://quantumvillage.org/>

[6] <https://github.com/QuantumVillage/UncutGem>

## Supplementary Material

### Background

A nitrogen vacancy (NV) center is a lattice defect in a diamond achieved by exchanging two carbon atoms with a nitrogen atom next to a lattice vacancy [1]. The NV center has several possible charge states, where the negatively charged state is often used as a qubit, mainly because of its spin and optical properties [2]. The basic effect which makes it possible to use NV centers for magnetometry is known as magnetic resonance. The principles behind this effect are often introduced in the context of electron paramagnetic resonance (EPR) spectroscopy. The type of resonance which is relevant for NV centers is optically detected magnetic resonance (ODMR). As the name suggests, the main difference between EPR and ODMR is the method of read-out for the resonance.

The intrinsic magnetic moment  $\boldsymbol{\mu}$  of the electron is given by

$$\boldsymbol{\mu} = -g_e\mu_B\hat{\mathbf{S}}, \quad (1)$$

where  $\hat{\mathbf{S}}$  is the spin operator,  $g_e$  is the  $g$ -factor for the free electron, and  $\mu_B$  is the Bohr magneton. In classical physics, the energy  $U$  of a magnetic moment in an applied magnetic field  $\mathbf{B}$  is

$$U = -\boldsymbol{\mu} \cdot \mathbf{B}. \quad (2)$$

This implies that if we neglect contributions from orbital angular momentum, we can promote the magnetic moment to an operator to obtain the Hamiltonian

$$H = -g_e\mu_B\hat{\mathbf{S}} \cdot \mathbf{B}. \quad (3)$$

If the magnetic field is aligned with the  $z$ -direction, the energy of the magnetic moment of the electron is given by

$$U = -g_e\mu_BBm_s, \quad (4)$$

where  $B$  is the magnitude of the magnetic field and  $m_s$  is the magnetic spin quantum number of the electron. Since the total spin quantum number  $S$  for an unpaired electron is  $+1/2$ , it follows that  $m_s$  can take either the value  $+1/2$  or  $-1/2$ , leading to two distinct energy levels, where the distance between the levels is given approximately by  $g_e\mu_BB$  (shown in Fig. 1 (left)). It can be seen that there is degeneracy when  $B = 0$  and that two energy levels form for  $B > 0$ , a phenomenon known as the Zeeman effect. If incident electromagnetic radiation (usually microwave radiation in this case) has an energy equal to the difference between the levels, absorption occurs. In EPR, one usually keeps the microwave frequency fixed and sweeps the magnetic field strength, whereas the microwave frequency is usually swept in

ODMR [3, 4]. The basic physics discussed above also applies to the NV center as a spin-1 state, although there are various complicating factors, such as the zero-field and hyperfine interactions. The  $g$ -factor (or more specifically, the gyromagnetic ratio) for the electron is used in calculations for NV centers (for example, in obtaining the sensitivity result which we present in Section III).

In Fig. 1 (right), we show the electronic energy level structure for the  $\text{NV}^-$  center, which has electron spin  $S = 1$  [5]. The ground  $^3A_2$  and excited  $^3E$  energy levels shown in the figure are spin-triplet states which split into spin sub-levels with  $m_s = 0$  and  $m_s = \pm 1$ , where the axis for the spin quantization is taken to be the symmetry axis which connects the substitutional nitrogen atom with the lattice vacancy [6, 7, 8]. There are also two spin singlets  $^1A_1$  and  $^1E$  [9, 10]. Electron interactions lead to a zero field splitting between the spin sub-levels in the ground state by  $D = 2.87$  GHz at room temperature, whereas the spin sub-levels for the first excited state are split by 1.42 GHz [11, 12].  $D$  can change depending on the temperature and varies as  $dD/dT = -74$  kHz  $\text{K}^{-1}$  at room temperature [13]. Magnetic dipole transitions with selection rules  $\Delta m_s = \pm 1$  can be stimulated using microwave radiation. The resonances can then be read out using EPR or ODMR.

In this article, we use the standard method of ODMR with a sweep through microwave frequencies, where two resonances appear in the spectrum due to the splitting of the  $m_s = \pm 1$  spin levels by the Zeeman effect [14, 15, 16, 17]. In the regime of sufficiently weak (but not too weak) magnetic fields, the splitting of the sub-levels is proportional to the projection of the magnetic field along the symmetry axis for the NV center [8]. This gives resonance frequencies in the ODMR spectrum equal to  $(2.87 \pm \gamma_e B_{\text{NVC}})$  GHz, where  $\gamma_e \approx 28$  GHz/T is the gyromagnetic ratio and  $B_{\text{NVC}}$  is the projection of the magnetic field along the symmetry axis of the NV center.

It follows that the splitting between the two resonant peaks in the spectrum is given by  $2\gamma_e B_{\text{NVC}}$ . Since the NV center can be oriented in four ways along its symmetry axis, a total of eight resonances can often be seen when the microwave frequency is swept. It is also possible to apply the magnetic field in certain orientations so that some of the resonances sit on top of each other. If the field is aligned along the  $[1\ 0\ 0]$  orientation, the projection of the field along a symmetry axis is the same for all four alignments of the NV center, so that the four resonances for each side collapse into one, and only two resonant peaks are observed.

The specific protocol which we use in our experiment is continuous-wave ODMR (cw-ODMR), where an ensemble of many NV centers in the diamond are all continuously illuminated with a green laser at the same time and driven with microwaves [17]. This work could be extended to demonstrate pulsed ODMR. An applied field known as the bias field with a strength between 1 and 10 mT lifts the degeneracy of the spin sub-levels and a magnetic object then causes the ODMR resonance frequencies to shift relative to the values set by the field. A microwave frequency is fixed to a resonance frequency for the ODMR and additional fields cause a shift in the resonance frequency, which is observed as a change in the fluorescence. Since the signal is extremely weak, one usually enhances the signal-to-noise ratio with phase-sensitive detection via a lock-in amplifier (the role of the LIA in our experiment will be played by a portable device called a Red Pitaya).

# LED Magnetometer

## Design

In this section, we discuss the components used to build the magnetometer (these are listed in Table I along with the model, estimated cost, and suggested supplier). The prices were checked on 22nd November 2025 and there may be some variation among different vendors. It is also possible to lower the cost by looking for used parts. The overall estimated cost of the device is around \$4500, similar to the setup described in [18]. In some cases, cheaper alternatives can be used to decrease the cost (for example, filtered glass could be used instead of a dichroic shortpass filter). We also expect that some re-design of the LED part could result in a substantial price reduction.

The only two components which are not 'off the shelf' are the metal wedge-shaped cornerpiece with two threaded holes for SM1 tubes and the circuit board with a metal pad on which the diamond sits. The former was machined in a workshop at the University of X and the latter was made by Eurocircuits. To aid anyone that is wishing to make a similar device, we include in the Supplementary Files technical drawings and CAD files that were used to make the circuit board. The metal pad is sized for the diamond which we use and is mainly for reflecting back fluorescence and excitation light. Aside from this component, the setup is relatively straightforward.

We used a 3 mm<sup>2</sup> CVD NV diamond from Element Six which had been irradiated and annealed. Suitable NV diamonds for the LED magnetometer could include DNV-B1 and DNV-B14 from Element Six, both of which cost around \$2000. The diamond is mounted on a standard PCB pad composed of copper with a thin nickel-gold (ENIG) finish, a non-magnetic surface which does not affect the applied bias field or the ODMR measurement. It may also be possible to use yellow diamonds if the user is able to anneal and irradiate them, where irradiation is needed to make vacancies (line widths will be broad but they should still function). For reference, vacancies become mobile above 800°. Typically, an inert atmosphere is used and the diamonds are buried in diamond grit, with annealing generally being carried out for 3 hours at 1000° C. This temperature is high enough for good mobility but low enough that the NV complex is stable. We provide a specific model for the SMA cables and the BNC converters used in the device, but we do not provide information on other miscellaneous screws, nuts or cables since these are readily available and the cables are recommended with the associated component by the supplier or sold with the component in question.

In constructing the device, we begin by securing the diamond to the metal pad on the circuit board with optical adhesive. The prism is placed on top of the diamond using optical adhesive. After this, the green LED and the longpass filter are threaded to the metal cornerpiece along with their respective SM1 tubes, where the LED is connected to the hexagonal light mixing rod. Since emission from the diamond is not focussed, the mixing rod helps to guide the emission to the photodetector and also gives distance between the electronics and the diamond. The cornerpiece is then placed down onto the circuit board so that the face of the light mixing rod is pressing up against the face of the prism, ready to direct light onto the diamond to reduce loss compared to an air-diamond interface. Ideally, during this phase one should use optical adhesive to sandwich the shortpass filter between



the face of the rod and the face of the prism. However, we found the process of fitting the shortpass filter in this way to be difficult and that the filter did not have much of an effect on the sensitivity of our device, so we suggest that this step could be skipped.

The design could also be improved so that the shortpass filter can be installed more easily. If this stage is followed, one will also need a glass scribe or diamond scribe to score and break the filter into a piece that fits against the face of the rod, but this is cheaply available at Thorlabs or a similar supplier. If full "slabs" of filter are used, more light may be directed out of the path via total internal reflection within the slab. At this stage, one can remove the SM1 tube for the longpass filter, turn on the green LED, and observe that red light is coming from the prism via the filter. Green light can be seen leaking out of the side of the device. This could be part of a demonstration, as it shows that the green light from the LED and the red fluorescence can be seen directly.

The SM1 tube with the longpass filter is screwed to the amplified photodetector. The device then naturally sits on top of the photodetector like a stand. A neodymium block magnet is attached to the upper right and bottom left corners of the circuit board using blu-tack so that both magnets sit flat against the board. These magnets provide the external bias field, which can be adjusted by changing the position and orientations of the magnets. A laptop is connected to the Red Pitaya STEMLab using a dongle. The Red Pitaya is a Xilinx Zynq-based combined FPGA and ARM system on chip (SoC) with capability as a portable USB oscilloscope. Custom-made Python software enables the Red Pitaya to be used as a lock-in amplifier and users wishing to implement the digital lock-in detection and automated microwave scans can consult the scripts provided in [19]. The first input port of the Red Pitaya is connected to the output of the photodetector using an SMA cable with a BNC converter. The first output port of the Red Pitaya is connected to the FM input of the microwave source, also with an SMA cable and a BNC converter. The custom-made circuit board is connected to the radio frequency output of the microwave source with a right-angle SMA cable. The LED driver is connected to the other port of the photodetector and the USB port of the microwave source is connected to the Red Pitaya with a USB cable.

## Sensitivity

In Fig. 2, we plot the sensitivity of the device as a function of frequency. The main motivation for this was to see how effective the device is given its simplicity. It is also of pedagogical interest to teach about sensitivity and parameter optimization. As expected, the sensitivity of the device is poor in comparison with more cutting-edge NV magnetometers, with a noise floor of  $1 \mu\text{T}/\sqrt{\text{Hz}}$ . However, this value is reasonable given the simplifications made with the design of the magnetometer and the fact that a laser was not used. Since no ODMR contrast is available when the microwaves are off-resonance or when the LED is turned off, the derived sensitivity in those cases represents the measurement noise floor rather than a physical magnetic field sensitivity. The signal at 50 Hz is due to the main power for electrical equipment in the lab.

Table 1: Suggested components for the LED magnetometer.

Component	Model	Estimated Cost	Supplier
Red Pitaya STEMLab	125-14	\$400	Red Pitaya
Microwave source	TPI-1005-A	\$300	RF Consultant
Dichroic 600 nm shortpass filter	69-180	\$100	Edmund Optics
Amplified photodetector	PDA100A2	\$400	Thorlabs
T-Cube LED driver	LEDD1B	\$300	Thorlabs
Small neodymium cube magnet $\times 2$	BA192	\$20	Sigel
Optical adhesive	NOA 61	\$30	Norland
3 mm <sup>2</sup> CVD NV diamond	DNV-B1	\$2000	Element Six
SM1 tube $\times 2$	SM1PL	\$20	Thorlabs
Green LED	M530L4	\$250	Thorlabs
Cornerpiece with two SM1 threads	CAD file	\$20	Workshop
Circuit board for diamond	CAD file	\$300	Eurocircuits
Hexagonal light mixing rod	HMR425	\$100	Thorlabs
NBK7 right angle optical prism	45-948	\$70	Edmund Optics
638 nm longpass filter	DMLP638T	\$100	Thorlabs
SMA cable $\times 2$	047-12SMPSM+	\$20	Minicircuits
Power supply for photodetector	LDS12B	\$70	Thorlabs
Right-angle SMA cable	ACX1611-ND	\$20	Digikey
SMA to BNC converter $\times 2$	242102	\$10	Digikey

## Example Labs

The magnetometer can be used in undergraduate labs to do quantitative analysis with ODMR spectra. For example, one can view the ODMR spectrum on the Red Pitaya user interface and alter the bias field until a  $[1\ 0\ 0]$  orientation is found [19]. This can be done by placing the two block magnets at opposite corners of the circuit board and rotating them by small amounts until two resonance peaks are seen. As a useful exercise, the strength of the bias field can be found using the equation for the frequency difference between two resonances  $\Delta = 2\gamma_e B_z$  after accounting for the projection factor of 0.58 for the  $[1\ 0\ 0]$  orientation. In our case, this gives  $B_z \approx 2.5\text{ mT}$ .

There are various ways that the magnetometer we developed could be studied further and used in projects for undergraduate labs. We offer some suggestions and advice below:

- Better understanding of the physics of the LED. Relationship between the power of the LED and fluorescence. Measurement and calibration of the LED power with regards to where the dial is positioned on the LED driver.
- Parameter optimization (LED power, microwave power, modulation frequency, modulation depth). Link between the physics of the NV center, pumping and optimization. This is useful to understand how a lock-in amplifier works.
- Can the bias field be adjusted to find orientations apart from  $[1\ 0\ 0]$ ? Is it possible to obtain orientations in which all eight peaks can be seen. This would be an easy exercise

to introduce in a lab since it only involves experimenting with different positions of the block magnets on the magnetometer and inspecting the ODMR spectrum on the Red Pitaya user interface. To achieve a  $[1\ 1\ 1]$  orientation, it may be necessary to fix the magnets at an angle so that they no longer sit flat on the circuit board.

- Can the design of the magnetometer be improved and made more compact? What are the physical limitations involved in doing this and does this worsen the sensitivity? As an example, can an LED be incorporated directly into the circuit board (this would reduce the cost of the device further) [20].
- What happens when the magnetometer is rotated in the Earth’s magnetic field?

## References

- [1] M.W. Doherty, N.B. Manson, P. Delaney, F. Jelezko, J. Wrachtrup and L.C. Hollenberg, The nitrogen-vacancy colour centre in diamond, *Phys. Rep.* **528**, 1 (2013).
- [2] N. Aslam, G. Waldherr, P. Neumann, F. Jelezko, and J. Wrachtrup, Photo-induced ionization dynamics of the nitrogen vacancy defect in diamond investigated by single-shot charge state detection, *New J. Phys.* **15**, 013064 (2013).
- [3] D. Goldfarb and S. Stoll, *EPR spectroscopy: fundamentals and methods* (John Wiley & Sons, 2018).
- [4] A. Schweiger and G. Jeschke, *Principles of pulse electron paramagnetic resonance* (Oxford University Press, 2001).
- [5] K. Jensen, P. Kahayias and D. Budker, Magnetometry with nitrogen-vacancy centers in diamond. In *High sensitivity magnetometers*, 553-576 (Springer, 2017).
- [6] J. Loubser and J. van Wyk, Electron spin resonance in the study of diamond, *Rep. Prog. Phys.* **41**(8), 1201 (1978).
- [7] N. R. S. Reddy, N. B. Manson and E. R. Krausz, Two-laser spectral hole burning in a colour centre in diamond, *J. Lumin.* **38**, 46–47 (1987).
- [8] L. Rondin, J. P. Tetienne, T. Hingant, J. F. Roch, P. Maletinsky, and V. Jacques, Magnetometry with nitrogen-vacancy defects in diamond. *Rep. Prog. Phys.* **77**(5), 056503 (2014).
- [9] L. J. Rogers, S. Armstrong, M. J. Sellars and N. B. Manson, Infrared emission of the NV centre in diamond: Zeeman and uniaxial stress studies, *New J. Phys.* **10**, 103024 (2008).
- [10] V. M. Acosta, A. Jarmola, E. Bauch, and D. Budker, Optical properties of the nitrogen-vacancy singlet levels in diamond, *Phys. Rev. B* **82**, 201202 (2010).
- [11] G. D. Fuchs, V. V. Dobrovitski, R. Hanson, A. Batra, C. D. Weis, T. Schenkel, and D. Awschalom, Excited-state spectroscopy using single spin manipulation in diamond, *Phys. Rev. Lett.* **101**, 117601 (2008).

- [12] P. Neumann, R. Kolesov, V. Jacques, J. Beck, J. Tisler, A. Batalov, L. Rogers, N. B. Manson, G. Balasubramanian, F. Jelezko, and J. Wrachtrup, Excited state spectroscopy of single NV defects in diamond using optically detected magnetic resonance, *New J. Phys.* **11**, 013017 (2009).
- [13] V.M. Acosta, E. Bauch, M.P. Ledbetter, A. Waxman, S. Bouchard and D. Budker, Temperature Dependence of the Nitrogen-Vacancy Magnetic Resonance in Diamond, *Phys. Rev. Lett.* **106**, 209901 (2011). Erratum, *Phys. Rev. Lett.* **106**, 209901 (2011)
- [14] J. M. Taylor, P. Cappellaro, L. Childress, L. Jiang, D. Budker, P. R. Hemmer, A. Yacoby, R. Walsworth, and M. D. Lukin. High-sensitivity diamond magnetometer with nanoscale resolution, *Nat. Phys.* **4**(10), 810–816 (2008).
- [15] G. Balasubramanian, I. Y. Chan, R. Kolesov, M. Al-Hmoud, J. Tisler, C. Shin, C. Kim, A. Wojcik, P. R. Hemmer, A. Krueger, T. Hanke, A. Leitenstorfer, R. Bratschitsch, F. Jelezko, and J. Wrachtrup, Nanoscale imaging magnetometry with diamond spins under ambient conditions, *Nature* **455** (7213), 648–651 (2008).
- [16] J. R. Maze, P. L. Stanwix, J. S. Hodges, S. Hong, J. M. Taylor, P. Cappellaro, L. Jiang, M. V. G. Dutt, E. Togan, A. S. Zibrov, A. Yacoby, R. L. Walsworth, and M. D. Lukin, Nanoscale magnetic sensing with an individual electronic spin in diamond, *Nature* **455** (7213), 644–647 (2008).
- [17] J. F. Barry, J. M. Schloss, E. Bauch, M. J. Turner, C. A. Hart, L. M. Pham, and R. L. Walsworth, Sensitivity optimization for NV-diamond magnetometry, *Rev. Mod. Phys.* **92** (1), 015004 (2020).
- [18] H. Zhang, C. Belvin, W. Li, J. Wang, J. Wainwright, R. Berg and J. Bridger, Little bits of diamond: Optically detected magnetic resonance of nitrogen-vacancy centers, *Am. J. Phys.* **86**, 225-236 (2018).
- [19] G.A. Stimpson, M.S. Skilbeck, R.L. Patel, B.L. Green and G.W. Morley, An open-source high-frequency lock-in amplifier, *Rev. Sci. Instrum.* **90**, 094701 (2019).
- [20] J. Pogorzelski, L. Horsthemke, J. Homrighausen, D. Stiegekoetter, M. Gregor and P. Gloesekoetter, Compact and Fully Integrated LED Quantum Sensor Based on NV Centers in Diamond, *Sensors* **2024** 24(3), 743 (2024).

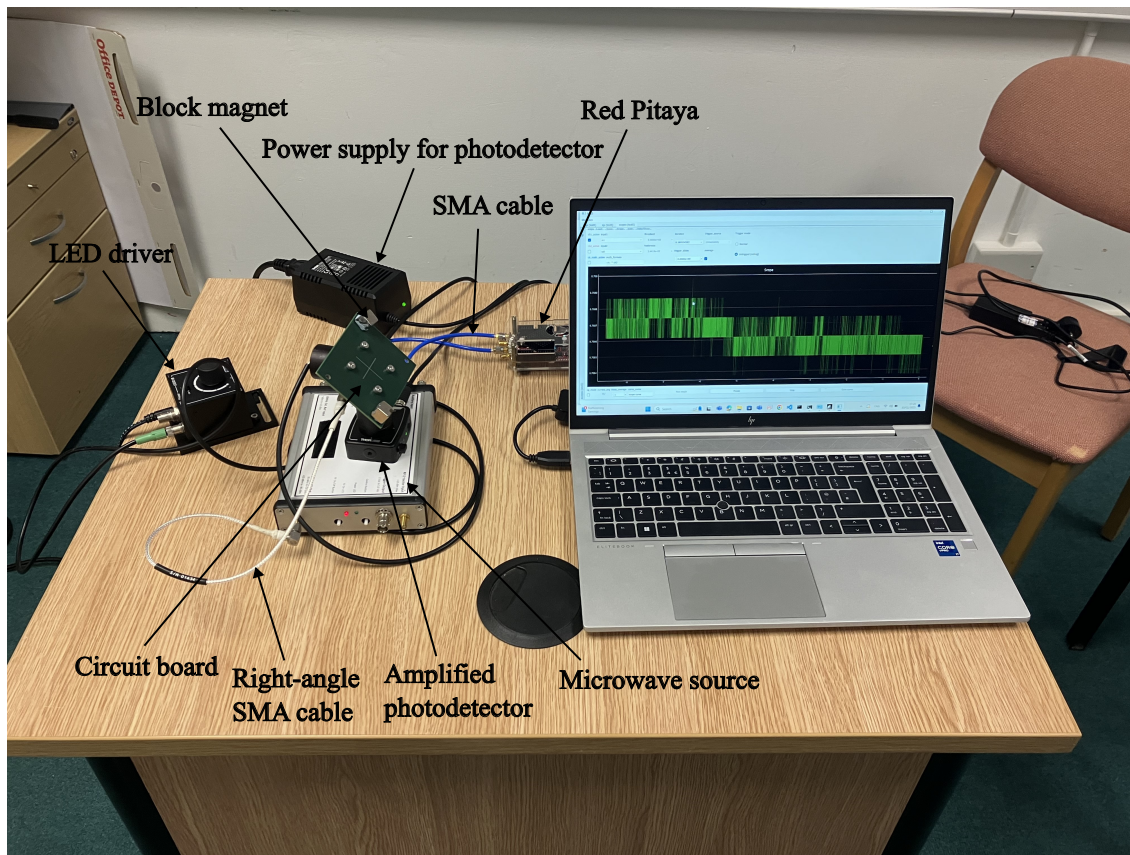


Figure 4: Photo of the demonstration setup.

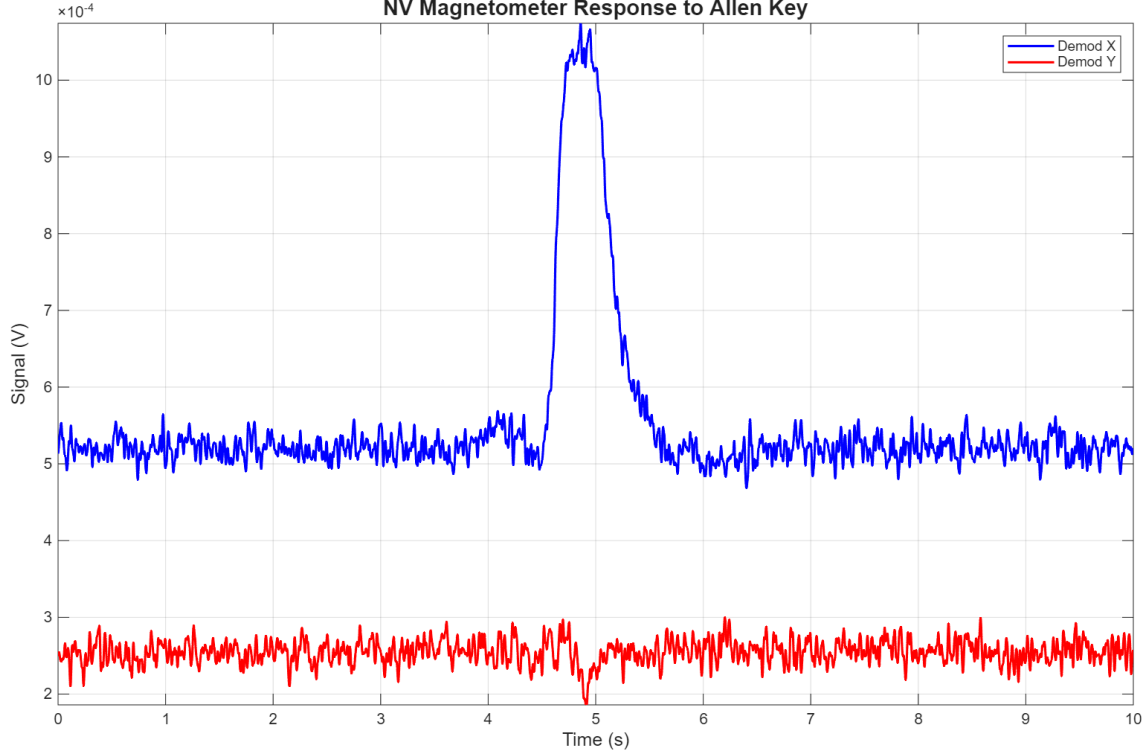


Figure 5: Time series of the demodulated PL signal when a steel Allen key is moved close to the magnetometer. The in-phase (“demod-X”) channel exhibits a spike, whereas the quadrature (“demod-Y”) channel remains near zero as expected for correctly phased lock-in detection. This measurement was performed using the LED magnetometer in its standard demonstration configuration.

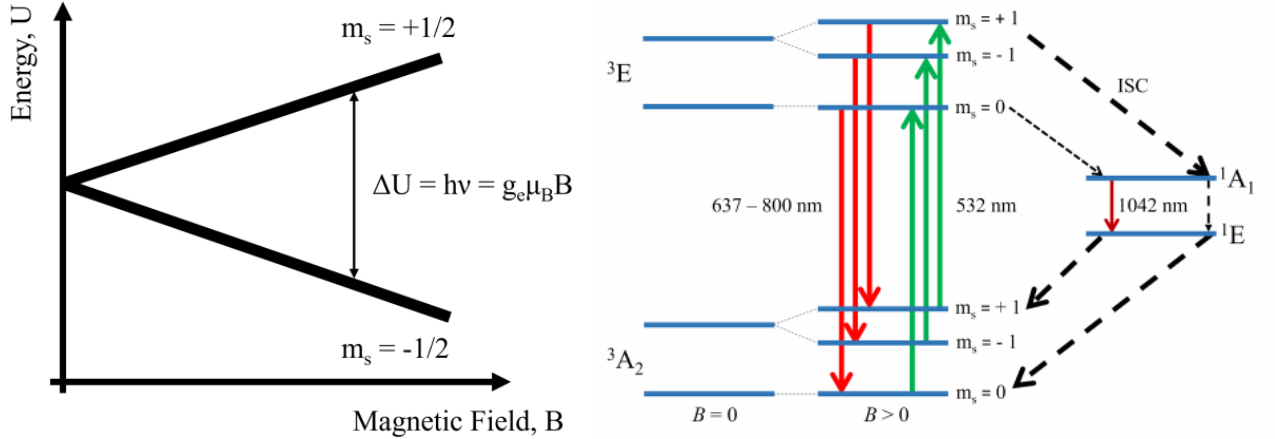


Figure 6: (Left) diagram for a spin-1/2 electron in an applied magnetic field  $B$  showing splitting of energies between the  $m_s = +1/2$  and  $m_s = -1/2$  spin sub-levels and (right) schematic of the NVC electronic structure, with intersystem crossings and electric dipole transitions shown.

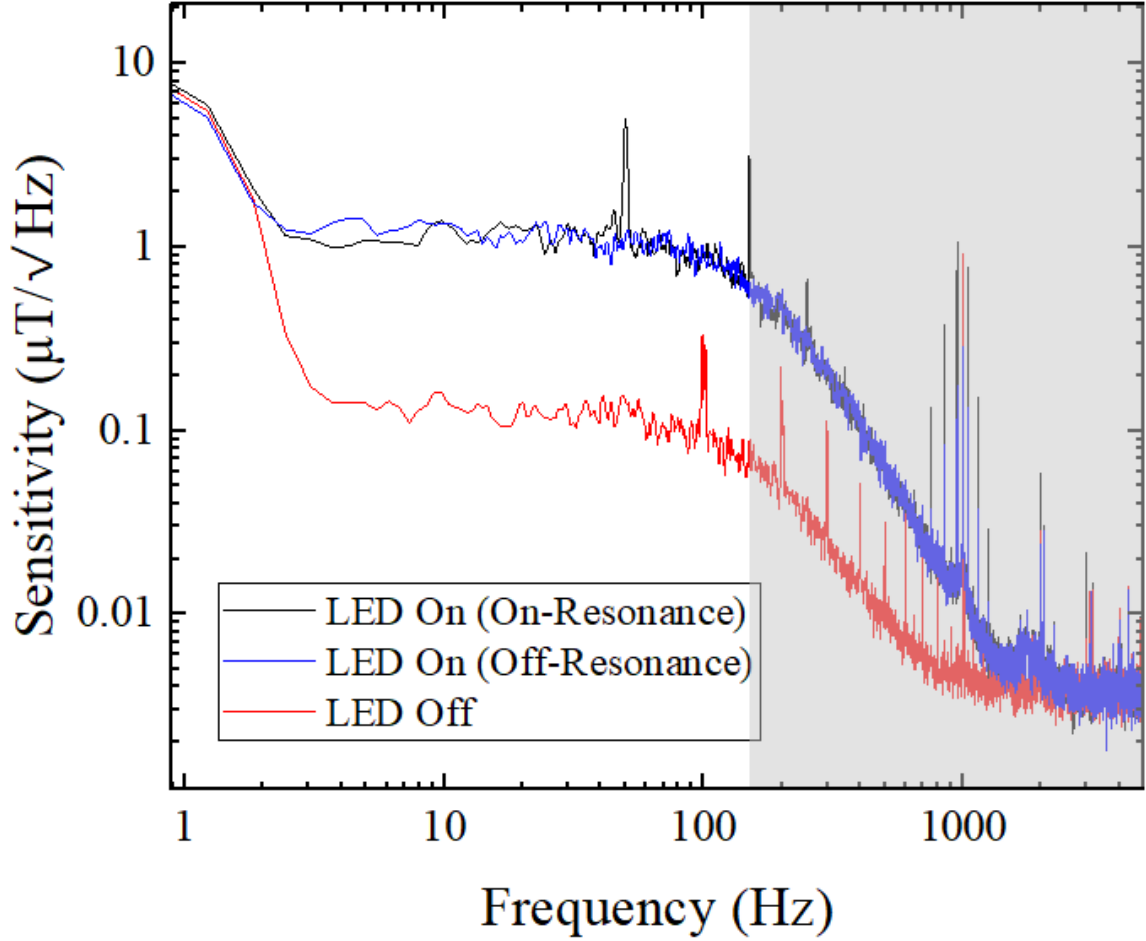


Figure 7: Plot of frequency vs sensitivity for the LED magnetometer. The black and blue lines indicate the result when the microwave driving is done at the frequency of a resonant peak and far away from a peak, respectively. With the LED turned off, the ODMR contrast vanishes and the sensitivity curve simply reflects the electronic noise floor of the detection chain. The lock-in amplifier is set to reject everything above around 100 Hz using a lock-in time constant of 10 ms. This means the equipment is not sensitive at frequencies above around 100 Hz, hence we have shaded this region of the plot gray.